Lithium-assisted exfoliation of pristine graphite for few-layer graphene nanosheets

Minwei Xu[1,2], Huiting Sun[1], Cai Shen[3], Sen Yang[1], Wenxiu Que[2], Yin Zhang[4] (✉), and Xiaoping Song[1] (✉)

[1] MOE Key Laboratory for Nonequilibrium Synthesis and Modulation of Condensed Matter, Xi'an Jiaotong University, Xi'an, 710049, China
[2] Electronic Materials Research Laboratory, International Center for Dielectric Research, Xi'an Jiaotong University, Xi'an 710049, China
[3] Ningbo Institute of Materials Technology and Engineering, Chinese Academy of Sciences, Ningbo, 315201, China
[4] School of Materials Science and Engineering, Tongji University, Shanghai, 201804, China

ABSTRACT

A lithium-assisted approach has been developed for the exfoliation of pristine graphite, which allows the large-scale preparation of few-layer graphene nanosheets. The process involves an unexpected physical insertion and exfoliation, and the graphene nanosheets prepared by this method reveal undisturbed sp^2-hybridized structures. A possible two-step mechanism, which involves the negative charge being trapped around the edges of the graphite layers and a subsequent lithiation process, is proposed to explain the insertion of lithium inside the graphite interlayers. If necessary, the present exfoliation can be repeated and thinner (single or 2–3 layer) graphene can be achieved on a large scale. This simple process provides an efficient process for the exfoliation of pristine graphite, which might promote the future applications of graphene.

KEYWORDS

graphene,
few-layer,
lithium Intercalation,
exfoliation

1 Introduction

Graphene, a single layer of carbon atoms in a honeycomb lattice, has been at the forefront of the scientific community since its discovery in 2004 [1–4]. It offers a number of fundamentally exceptional properties that make it a promising material for a wide range of applications including electronic devices [5–8], transparent conductive films [9, 10], energy storage [11–14], and biosensors [15]. As the first step to realize these applications, however, the mass production of high-quality graphene nanosheets remains a great challenge. To date, numerous methods have been developed to produce graphene nanosheets, such as mechanical exfoliation [1], reduction of graphene oxide [16, 17], liquid-phase exfoliation [18, 19], chemical vapour deposition [20], epitaxial growth on SiC substrates [21], electrochemical exfoliation [22, 23] and organic synthesis [24]. However, these synthetic methods usually lack one or more of the following attributes: (1) Products with undisturbed sp^2-hybridized structures; (2) high throughput and low cost; (3) controllability over layer number, size and shape; (4) low energy consumption; and (5) mild processes.

Address correspondence to Yin Zhang, yzhang18@tongji.edu.cn; Xiaoping Song, xpsong@mail.xjtu.edu.cn

Thus, many challenges remain and the foremost target is to develop the alternative methods for the large-scale synthesis of graphene nanosheets.

Inspired by the electrochemical reactions of negative graphite electrodes in lithium ion batteries (LIBs), we believe that the exfoliation of lithium intercalated graphite can give rise to single- or few-layer graphene nanosheets. For example, Zhang et al. developed a universal lithiation process to fabricate single-layer 2D nanomaterials [25], which has potential significance to advance the fabrication of high-quality graphene nanosheets. However, in their work lithium intercalation was performed in a test cell, where a Li foil anode and electrolyte were needed. The complexity of the electrochemical intercalation process and the limited throughput limit the applicability of this method. Herein, based on the lithium intercalation concept, we demonstrate a simple approach to producing ultrathin graphene nanosheets in large yield and with high quality by lithium-assisted exfoliation of bulk graphite minerals.

2 Experimental

Liquid ammonia was selected as the solvent since metallic lithium can be dissolved in anhydrous ammonia. The simple and reproducible exfoliation was performed as follow: Initial bulk graphite (30 mg) was added to a flame-dried 100 mL flat bottom flask. Liquid ammonia (about 60 mL) was then cooled and condensed into the flask, followed by addition of 300 mg of lithium metal. The deep blue colored composites were magnetically stirred for 2 h with the temperature maintained at about –33 ℃ by means of an acetone/dry ice bath. The bath was removed after 2 h and the reaction continued overnight with slow evaporation of ammonia. Then, 200 mL of dilute HCl solution was added into flask while mild sonication was applied. Finally, the black products were cleaned by filtration several times and finally dispersed in ethanol. After a slow centrifugation, the supernatant dispersion was collected for the further characterization. The resulting graphene nanosheets display a good stability of their dispersion in ethanol. The present exfoliation is easily reproducible and we believe that that thinner graphene nanosheets can be achieved.

3 Results and discussion

Liquid ammonia is an ionizing solvent. It can dissolve metallic lithium to form a deep blue solution, which is widely used for hydrogenation of aromatic hydrocarbons and various carbon allotropes [26–29]. In this work, we used this Li/liquid ammonia solution to synthesize a lithium intercalated graphite precursor in order to obtain few-layer graphene nanosheets on a large scale. The overall processes are illustrated in Fig. 1. The Li/liquid ammonia solution is a strong reducing agent and reacts with graphite to form the well-known [graphite anion]$^{-}$Li^{+} composites [30]. As a result, the graphene layers of the graphite become negatively charged and the van der Waals forces between the stacked graphene layers are overcome. More importantly, the charged points tend to occur around the defect sites of graphene interlayers, whilst maintaining the majority of the pristine sp^2 structure [31]. This means that the Li^{+} ions are likely to aggregate at the edges of the graphite sheets, since the edges show much higher defect density. Such aggregation will expand the edges of the graphite layers and open a channel to facilitate the insertion of Li inside the graphite. When the liquid ammonia was evaporated slowly, as shown in Fig. S1 in the Electronic Supplementary Material (ESM), the color of the solution changed from blue to brilliant bronze due to

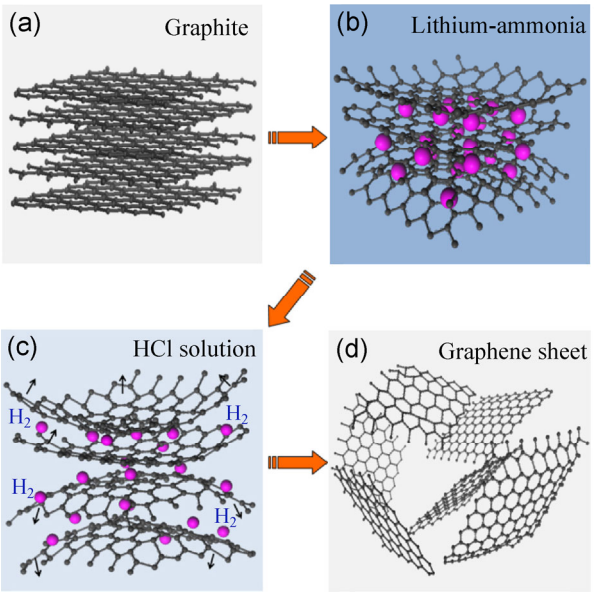

Figure 1 Schematic illustration of the lithium-assisted exfoliation of bulk graphite minerals.

the increasing concentration. Meanwhile, the lithium intercalated graphite is formed spontaneously (Fig. 1(b)). The subsequent acid treatment allows the intercalated Li to react with HCl solution. The resulting release of H_2 is able to lead to exfoliation, which further unwraps the graphite layers and forces them apart (Fig. 1(c)). This exfoliation will completely destroy the pristine graphite stacking structure, finally affording graphene nanosheets (Fig. 1(d)).

As revealed in Fig. 2, the starting bulk graphite showed a very disordered and irregular appearance with an average particle size of 150 μm (Fig. 2(a)) and it was used as received. As shown in a representative Scanning Electron Microscope (SEM, JEOL JSM-7000F) image (Fig. 2(b)), the as-produced graphene showed a wrinkled morphology, which suggested that almost all the graphite powder had been exploded into pieces of soft graphene nanosheets. These graphene nanosheets were clearly observed without any charging problems. Figures 2(c) and S2 (in the ESM) reveal the individual nanosheets, which are spread on the substrate and have a wrinkled appearance. By mild sonication, these graphene nanosheets can be well dispersed in ethanol (Fig. 2(d)). Figure S3 (in the ESM) shows the graphite and graphene nanosheet suspensions, after being kept quiescent overnight. An obvious volume expansion is revealed, which demonstrates the exfoliation of the graphite. Moreover, the supernatant of the graphene suspension displays a typical Tyndall effect, suggesting the formation of stable graphene nanosheets. The exfoliation of the graphite can also be demonstrated by X-ray diffraction (XRD). As shown in Fig. S4 (in the ESM), the intensity of the sharp diffraction peak of graphite ($2\theta = 26.5°$, corresponding to the interlayer distance (0.336 nm)) decreased dramatically. No new diffraction peaks for graphene oxide or other impurities appeared, indicating the exfoliation of graphite.

Transmission Electron Microscope (TEM, JEOL JEM-2100) was then carried out to further identify and characterize the degree of exfoliation and quality of graphene. The TEM sample was prepared by directly dropping the supernatant of the graphene suspension

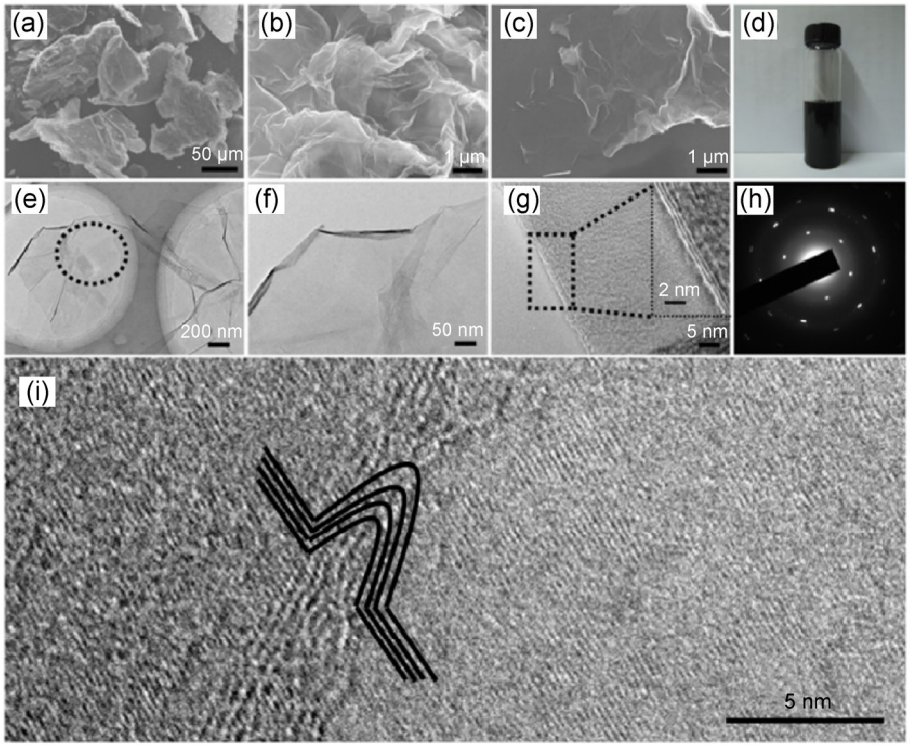

Figure 2 SEM images of (a) bulk graphite, (b) as-produced graphene and (c) an individual graphene nanosheet. The entire image (b) consists of massive individual graphene nanosheets assembled into a flower-like structure with cavities, edges or wrinkles. (d) A photograph of a graphene nanosheet dispersion in ethanol. (e)–(g) TEM images and (inset and (i)) HRTEM image of graphene nanosheets. (h) The SAED pattern originating from the marked area in (e).

in ethanol onto a Cu grid. In Figs. 2(e) and 2(f), large thin graphene sheets can be observed on the top of the Cu grid, where they resemble crumpled silk veil waves. The edges of the graphene sheets tend to scroll and fold, which is regarded as an intrinsic property of graphene. The graphene nanosheets are transparent and exhibit a very stable nature under electron beam. Since the suspended sheets always wrinkle, this offers a means to reveal the layer number of graphene by using high magnification TEM (HRTEM). As shown in Fig. 2(g). triple layers of graphene nanosheets were identified in the corrugated regions. Figure 2(i) exhibits a typical folded feature in the middle of a graphene nanosheet. As illustrated, four-layer graphene appears to be folded in the center. The planar lattice can be clearly resolved in the ordered crystal structure. The distinctive lattice structure reveals that the high-quality graphene sheets maintained their structural integrity without significant defects. The selected area electron diffraction (SAED) pattern confirms the hexagonal 2D crystal structure of our products. More graphene images and layer detail can be found in Fig. S5 (in the ESM).

Figure 3 shows the Atomic Force Microscope (AFM, Agilent 5500) images of isolated graphene nanosheets which were prepared by spin coating from a dilute ethanol solution on freshly cleaved mica. The representative image exhibits a lateral dimension ranging from several hundred nanometers to micrometers and a uniform thickness of ~1.1 nm, corresponding to 2–3 layers of graphene. The AFM images confirm that the dispersion contains isolated graphene nanosheets with ultrathin thickness.

Raman spectroscopy has historically played a significant role in characterizing carbon allotropes, and is widely used in studying the defects in graphene nanosheets. The G peak located at ~1,580 cm^{-1} and 2D (G′) peak at ~ 2,700 cm^{-1} arise from in-plane vibrations of sp^2 carbon atoms and second-order zone boundary phonons, respectively. The D band is stimulated by the first-order zone boundary phonons, which result from the presence of defects or edge effects of graphene [32]. The Raman spectrum of our pristine bulk graphite displays a weak D peak at 1,336 cm^{-1}, a strong G peak at 1,582 cm^{-1}, and a 2D peak at 2,727 cm^{-1}. For the graphene nanosheets, an increased intensity of the D peak and the appearance of a new peak (at 1,610 cm^{-1}) near the G band are observed. The new peak is denoted the D′ peak, and also arises from disorder (Fig. 4 inset). Our synthesis method does not remove carbon atoms from the graphene lattice [33]. Thus, the appearance of the D′ peak and the increased intensity of the D peak result mainly from functionalization of the graphene. Since the Raman excitation beam can cover a large number of graphene edges, we believe that the functionalization mainly occurs near the graphene edges. The lack of broadening G band also indicates that the disorder comes from the edges, rather than from structural defects within the graphene planes [34–36]. Figure 4(b) shows the Fourier transform infrared (FTIR) spectrum of the graphene nanosheets. The absorption bands near 2,850 cm^{-1} can be assigned to C–H stretching modes [37]. The presence of such C–H stretching modes, which are absent in the FTIR spectrum of pristine graphite, indicates the functionalization of graphene edge by hydrogen during the exfoliation process.

The main reaction responsible for the hydrogenation of graphite in Li/liquid ammonia systems is the

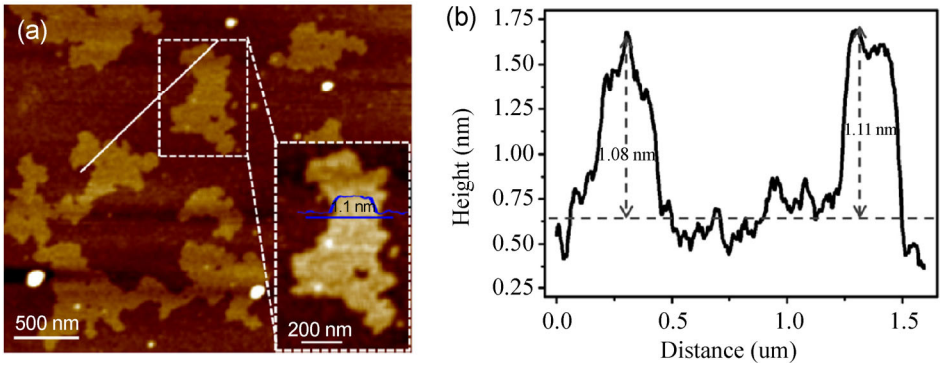

Figure 3 (a) AFM images of the obtained graphene nanosheets with (b) the corresponding height profile of a line scan.

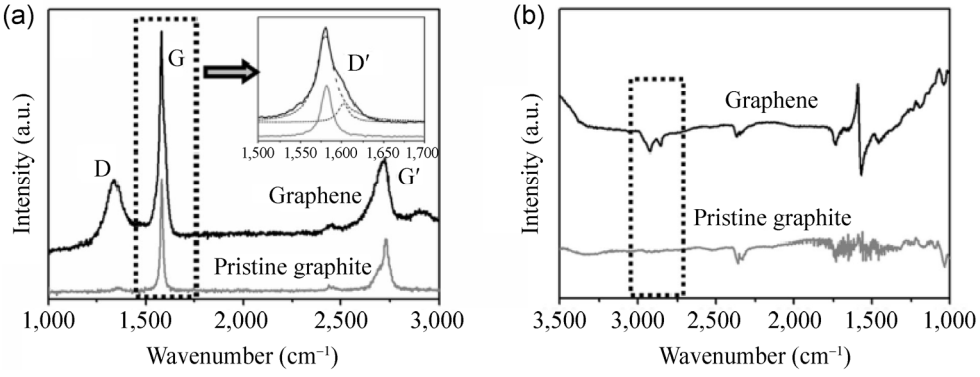

Figure 4 (a) Raman and (b) FTIR spectroscopy of the graphite and graphene nanosheets.

reaction of reduced graphite with proton sources, which involves a single-electron transfer from the graphenide sheets to the proton source forming H radicals [38]. Subsequent radical recombination reactions lead to the hydrogenation of graphene. The key prerequisite for high efficiency of graphene hydrogenation is that the proton source should be slowly added. The presence of a low local concentration of hydrogen radicals ensures the hydrogenation of graphene rather than their recombination to afford H_2. In our process, the rapid addition of HCl solution will quench the reaction rather than promote the hydrogenation of graphene. In addition, no other proton sources such as methanol, ethanol or tert-butyl alcohol are involved. Thus, we believe that the exfoliation is the dominant process, while the unavoidable adsorbed water molecules or the water molecules in air can cause a small amount of hydrogenation of graphene at the edge areas.

To investigate the stability of the graphene nanosheets, we performed thermogravimetric analysis and the results are shown in Fig. S6 (in the ESM). The graphene nanosheets show a slight weight loss up to 700 ℃ in N_2 atmosphere. In air, the major mass loss took place above 500 ℃ while a slight mass loss in the temperature range 200–400 ℃ can also be observed. Generally speaking, a weight loss below 400 ℃ can be attributed to the release of adsorbed species such as alcohol and ammonia [39]. For our materials, the extra mass loss for graphene nanosheets in air below 400 ℃ can be attributed to the decomposition of graphene nanosheets at the defect areas, such as the edges and hydrogenated areas. These defect areas are more reactive than an undistorted graphene lattice, and react with O_2 at lower temperature. However, the combustion of graphene at about 550 ℃ is still the dominant process, which is consistent with hydrogenated area being very limited.

It should be mentioned that it is well known that alkali metals form graphite intercalation compounds (GICs, such as KC_8, CsC_8) by mixing the molten alkali metals with graphite powder [40–42]. After the discovery of graphene, several groups attempted to prepare graphene by exfoliation of these GICs. However, to the best of our knowledge, such methods only achieved the graphite nanoplatelets rather than single or few-layer graphene [43]. Comparing these previous studies with our lithium-assisted exfoliation, we suggest that the formation of [graphite anion]$^-$Li$^+$ composites plays an important role in exfoliation since the negatively charged graphene layers can not only overcome the van der Waals's interplanar binding force but also facilitate the lithiation process leading to graphite intercalation compounds. As a result, the exfoliation efficiency can be significantly improved.

In order to gain a better understanding of the lithium-assisted exfoliation, a sodium-assisted exfoliation experiment, where lithium was replaced by sodium, was also investigated. The obtained products show relatively large flakes and very thick features (see Fig. S7 in the ESM), which is indicative of a low exfoliation efficiency. The probable reason why intercalated graphite is more readily formed when Li is used as the intercalant is due to the large size of the sodium ion. Thus, the activation energy for sodium access should be much higher and the materials

contain less intercalated sodium, resulting an incomplete exfoliation. As a result, only graphene flakes could be obtained when sodium metal was used.

4 Conclusions

We have developed an effective and efficient method for the preparation of few-layer graphene nanosheets by lithium-assisted exfoliation of pristine graphite. The negatively charged graphene layers can not only overcome the van der Waals's interplanar binding force, but also facilitate the insertion of lithium into the graphite. Our exfoliation involves a mild physical treatment which maintains the honeycomb lattice. If necessary, the exfoliation process can be repeated and thinner (single or 2–3 layer) graphene can be achieved. These results may be useful for industrial-scale graphene preparation, and might promote the applications of graphene.

Acknowledgements

This work was supported by the National Natural Science Foundation of China (No. 51222104) and the Fundamental Research Funds for the Central Universities.

Electronic Supplementary Material: Supplementary material (photographs of the precursor and the obtained graphene nanosheets, XRD curves, Thermogravimetric Analysis (TGA, NETZSCH STA 449C JUPITER) curves and further SEM and TEM images for graphene nanosheets and graphene flakes) is available in the online version of this article at http://dx.doi.org/10.1007/s12274-014-0562-4.

References

[1] Novoselov, K. S.; Geim, A. K.; Morozov, S. V.; Jiang, D.; Zhang, Y.; Dubonos, S. V.; Grigorieva, I. V.; Firsov, A. A. Electric field effect in atomically thin carbon films. *Science* **2004**, *306*, 666–669.

[2] Geim, A. K.; Novoselov, K. S. The rise of graphene. *Nat. Mater.* **2007**, *6*, 183–191.

[3] Novoselov, K. S.; Fal'ko, V. I.; Colombo, L.; Gellert, P. R.; Schwab, M. G.; Kim, K. A roadmap for graphene. *Nature* **2012**, *490*, 192–200.

[4] Singh, V.; Joung, D.; Zhai, L.; Das, S.; Khondaker, S. I.; Seal, S. Graphene based materials: Past, present and future. *Prog. Mater. Sci.* **2011**, *56*, 1178–1271.

[5] Avouris, P.; Dimitrakopoulos, C. Graphene: Synthesis and applications. *Mater. Today* **2012**, *15*, 86–97.

[6] Wu, J. S.; Pisula, W.; Müllen, K. Graphene as potential material for electronics. *Chem. Rev.* **2007**, *107*, 718–747.

[7] Weiss, N. O.; Zhou, H. L.; Liao, L.; Liu, Y.; Jiang, S.; Huang, Y.; Duan, X. F. Graphene: An emerging electronic material. *Adv. Mater.* **2012**, *43*, 5782–5825.

[8] Bonaccorso, F.; Sun, Z.; Hasan, T.; Ferrari, A. C. Graphene photonics and optoelectronics. *Nat. Photon.* **2010**, *4*, 611–622.

[9] Wang, X.; Zhi, L. J.; Müllen, K. Transparent, conductive graphene electrodes for dye-sensitized solar cells. *Nano Lett.* **2008**, *8*, 323–327.

[10] Zhu, Y. W.; Murali, S.; Cai, W. W.; Li, X. S.; Suk, J. W.; Potts, J. R.; Ruoff, R. S. Graphene and graphene oxide: Synthesis, properties, and applications. *Adv. Mater.* **2010**, *22*, 3906–3924.

[11] Sun, Y. Q.; Wu, Q.; Shi, G. Q. Graphene based new energy materials. *Energy Environ. Sci.* **2011**, *4*, 1113–1132.

[12] Sahoo, N. G.; Pan, Y. Z.; Li, L.; Chan, S. H. Graphene-based materials for energy conversion. *Adv. Mater.* **2012**, *24*, 4203–4210.

[13] Xu, C. H.; Xu, B. H.; Gu, Y.; Xiong, Z. G.; Sun, J.; Zhao, X. S. Graphene-based electrodes for electrochemical energy storage. *Energy Environ. Sci.* **2013**, *6*, 1388–1414.

[14] Huang, X.; Qi, X. Y.; Boey, F.; Zhang, H. Graphene-based composites. *Chem. Soc. Rev.* **2012**, *41*, 666–686.

[15] Yang, W. R.; Ratinac, K. R.; Ringer, S. P.; Thordarson, P.; Gooding, J. J.; Braet, F. Carbon nanomaterials in Biosensors: Should you use nanotubes or graphene? *Angew. Chem. Int. Ed.* **2010**, *49*, 2114–2138.

[16] Hummers, W. S.; Offeman, R. E. Preparation of graphitic oxide. *J. Am. Chem. Soc.* **1958**, *80*, 1339–1339.

[17] Tung, V. C.; Allen, M. J.; Yang, Y.; Kaner, R. B. High-throughput solution processing of large-scale graphene. *Nat. Nanotechnol.* **2009**, *4*, 25–29.

[18] Lotya, M.; Hernandez, Y.; King, P. J.; Smith, R. J.; Nicolosi, V.; Karlsson, L. S.; Blighe, F. M.; De, S.; Wang, Z. M.; McGovern, I. T. et al. Liquid phase production of graphene by exfoliation of graphite in surfactant/water solutions. *J. Am. Chem. Soc.* **2009**, *131*, 3611–3620.

[19] Hernandez, Y.; Nicolosi, V.; Lotya, M.; Blighe, F. M.; Sun, Z. Y.; De, S.; McGovern, I. T.; Holland, B.; Byrne, M.; Gun'Ko, Y. K. et al. High-yield production of graphene by liquid-phase exfoliation of graphite. *Nat. Nanotechnol.* **2008**, *3*, 563–568.

[20] Li, X. S.; Cai, W. W.; An, J.; Kim, S.; Nah, J.; Yang, D. X.; Piner, R.; Velamakanni, A.; Jung, I.; Tutuc, E. et al. Large-area synthesis of high-quality and uniform graphene films on copper foils. *Science* **2009**, *324*, 1312–1314.

[21] Virojanadara, C.; Syväjarvi, M.; Yakimova, R.; Johansson, L. I.; Zakharov, A. A.; Balasubramanian, T. Homogeneous large-area graphene layer growth in 6H-SiC(0001). *Phys. Rev. B* **2008**, *78*, 245403.

[22] Su, C. Y.; Lu, A. Y.; Xu, Y. P.; Chen, F. R.; Khlobystov, A. N.; Li, L. J. High-quality thin graphene films from fast electrochemical exfoliation. *ACS Nano* **2011**, *5*, 2332–2339.

[23] Wang, J. Z.; Manga, K. K.; Bao, Q. L.; Loh, K. P. High-yield synthesis of few-layer graphene flakes through electrochemical expansion of graphite in propylene carbonate electrolyte. *J. Am. Chem. Soc.* **2011**, *133*, 8888–8891.

[24] Choucair, M.; Thordarson, P.; Stride, J. A. Gram-scale production of graphene based on solvothermal synthesis and sonication. *Nat. Nanotechnol.* **2009**, *4*, 30–33.

[25] Zeng, Z. Y.; Yin, Z. Y.; Huang, X.; Li, H.; He, Q. Y.; Lu, G.; Boey, F.; Zhang, H. Single-layer semiconducting nanosheets: High-yield preparation and device fabrication. *Angew. Chem. Int. Ed.* **2011**, *50*, 11093–11097.

[26] Vasil'ev, Y.; Wallis, D.; Nüchter, M.; Ondruschka, B.; Lobach, A.; Drewello, T. From major to minor and back—a decisive assessment of $C_{60}H_{36}$ with respect to the Birch reduction of C_{60}. *Chem. Commun.* **2000**, 1233–1234.

[27] Birch, A. J. Reduction by dissolving metals. Part I. *J. Chem. Soc.* **1944**, 430–436.

[28] Subrahmanyam, K. S.; Kumar, P.; Maitra, U.; Govindaraj, A.; Hembram, K. P. S. S.; Waghmare, U. V.; Rao, C. N. R. Chemical storage of hydrogen in few-layer graphene. *Proc. Natl. Acad. Sci. USA* **2011**, *108*, 2674–2677.

[29] Liang, F.; Sadana, A. K.; Peera, A.; Chattopadhyay, J.; Gu, Z. N.; Hauge, R. H.; Billups, W. E. A convenient route to functionalized carbon nanotubes. *Nano Lett.* **2004**, *4*, 1257–1260.

[30] Yang, Z. Q.; Sun, Y. Q.; Alemany, L. B.; Narayanan, T. N.; Billups, W. E. Birch reduction of graphite edge and interior functionalization by hydrogen. *J. Am. Chem. Soc.* **2012**, *134*, 18689–18694.

[31] Deng, S. L.; Zhang, Y.; Brozena, A. H.; Mayes, M. L.; Banerjee, P.; Chiou, W. A.; Rubloff, G. W.; Schatz, G. C.; Wang, Y. H. Confined propagation of covalent chemical reactions on single-walled carbon nanotubes. *Nat. Commun.* **2011**, *2*, 382.

[32] Dresselhaus, M. S.; Jorio, A.; Hofmann, M.; Dresselhaus, G.; Saito, R. Perspectives on carbon nanotubes and graphene Raman spectroscopy. *Nano Lett.* **2010**, *10*, 751–758.

[33] Sun, C. F.; Karki, K.; Jia, Z.; Liao, H. W.; Zhang, Y.; Li, T.; Qi, Y.; Cumings, J.; Rubloff, G. W.; Wang, Y. H. A beaded-string silicon anode. *ACS Nano* **2013**, *7*, 2717–2724.

[34] Liu, W. W.; Wang, J. N. Direct exfoliation of graphene in organic solvents with addition of NaOH. *Chem. Commun.* **2011**, *47*, 6888–6890.

[35] Ferrari, A. C.; Basko, D. M. Raman spectroscopy as a versatile tool for studying the properties of graphene. *Nat. Nanotechnol.* **2013**, *8*, 235–246.

[36] Casiraghi, C.; Hartschuh, A.; Qian, H.; Piscanec, S.; Georgi, C.; Fasoli, A.; Novoselov, K. S.; Basko, D. M.; Ferrari, A. C. Raman spectroscopy of graphene edges. *Nano Lett.* **2009**, *4*, 1433–1441.

[37] Krishna, R.; Titus, E.; Costa, L. C.; Menezes, J. C. J. M. D. S.; Correia, M. R. P.; Pinto, S.; Ventura, J.; Araujo, J. P.; Cavaleiro, J. A. S.; Gracio, J. J. A. Facile synthesis of hydrogenated reduced graphene oxide via hydrogen spillover mechanism. *J. Mater. Chem.* **2012**, *22*, 10457–10459.

[38] Schafer, R. A.; Englert, J. M.; Wehrfritz, P.; Bauer, W.; Hauke, F.; Seyller, T.; Hirsch, A. On the way to graphane—pronounced fluorescence of polyhydrogenated graphene. *Angew. Chem. Int. Ed.* **2013**, *52*, 754–757.

[39] Pekker, S.; Salvetat, J. P.; Jakab, E.; Bonard, J. M.; Forró, L. Hydrogenation of carbon nanotubes and graphite in liquid ammonia. *J. Phys. Chem. B* **2001**, *105*, 7938–7943.

[40] Chakraborty, S.; Chattopadhyay, J.; Guo, W. H.; Billups, W. E. Functionalization of potassium graphite. *Angew. Chem. Int. Ed.* **2007**, *46*, 4486–4488.

[41] Savoia, D.; Trombini, C.; Umani-Ronchi, A. Applications of potassium-graphite and metals dispersed on graphite in organic synthesis. *Pure Appl. Chem.* **1985**, *57*, 1887–1896.

[42] Matsumoto, R.; Akuzawa, N.; Takahashi, Y. Thermoelectric properties of cesium-graphite intercalation compounds. *Mater. Trans.* **2006**, *47*, 1458–1463.

[43] Viculis, L. M.; Mack, J. J.; Mayer, O. M.; Hahm, H. T.; Haner, R. B. Intercation and exfoliation routes to graphite nanoplatelets. *J. Mater. Chem.* **2005**, *15*, 974–978.